AIAA JOURNAL
Vol. 47, No. 11, November 2009

# Sound Generation by a Rotor Interacting with a Casing Turbulent Boundary Layer

David B. Stephens* and Scott C. Morris†
*University of Notre Dame, Notre Dame, Indiana 46556*

DOI: 10.2514/1.43271

**A new method for predicting the noise generated by a ducted rotor interacting with inhomogeneous and nonisotropic turbulence has been developed. The analytical formulation used a model of the two-point correlation function of the turbulent velocity in the space–time domain. The study focused on a specific condition where the dominant noise source was the interaction between a rotor and a casing turbulent boundary layer. The axial length scale of this turbulence was found to be large enough to generate unsteady lift that was correlated between multiple rotor blades. This led to tonal sound at the blade passing frequency in the absence of mean velocity variations. The analytical formulation was validated with a set of measurements obtained in a ducted rotor facility. The prediction accurately modeled both the tonal and broadband features of the sound spectra.**

## Nomenclature

| | | |
|---|---|---|
| $B$ | = | number of rotor blades |
| $C$ | = | rotor blade chord |
| $c$ | = | speed of sound |
| $D$ | = | duct diameter |
| $f$ | = | frequency, Hz |
| $k$ | = | acoustic wave number, $2\pi f/c$ |
| $\mathcal{L}$ | = | gust response function |
| $R$ | = | Boundary-layer dimensional two-point correlation of axial velocity |
| $R_{ww}$ | = | airfoil spanwise two-point correlation of upwash velocity between blades $m$ and $n$ |
| $r_{\text{tip}}$ | = | rotor tip radius |
| $s$, $s'$ | = | rotor blade span coordinate and corresponding dummy variable for integration |
| $\bar{U}$ | = | spatial mean axial velocity inside duct |
| $U_{\text{tip}}$ | = | tip relative fluid velocity, $V_{\text{tip}}\sqrt{1+\phi^2}$ |
| $\tilde{u}$ | = | unsteady axial velocity in casing reference frame |
| $\overline{\tilde{u}^2}$ | = | variance of axial velocity in casing reference frame |
| $V_{\text{tip}}$ | = | rotor tip velocity |
| $\hat{w}$ | = | Fourier transform of unsteady upwash velocity in rotor blade reference frame |
| $z$, $z_{\text{ref}}$ | = | boundary-layer wall-normal distance and reference location |
| $\alpha_y$, $\alpha_z$ | = | stretching parameter for spanwise and wall-normal directions |
| $\beta(\omega)$ | = | abbreviation for the combined variables, $\pi\rho CU\mathcal{L}(\omega)$ |
| $\Delta y$ | = | boundary-layer spanwise separation distance |
| $\theta$ | = | boundary-layer momentum thickness |
| $\rho$ | = | fluid density |
| $\tau$ | = | time lag for correlation functions |
| $\phi$ | = | flow coefficient, $\bar{U}/V_{\text{tip}}$ |
| $\psi$ | = | head rise coefficient, $2\Delta p/\rho V_{\text{tip}}^2$ |
| $\omega$ | = | angular frequency, $2\pi f$ |

Received 20 January 2009; accepted for publication 2 August 2009. 

*Postdoctoral Research Assistant, Department of Aerospace and Mechanical Engineering. Member AIAA.

†Associate Professor, Department of Aerospace and Mechanical Engineering. Member AIAA.

## I. Introduction

AXIAL flow ducted rotors are important in numerous engineering applications, ranging from ventilation equipment to jet engines. The noise generated by these systems often imposes limitations on their size or operation. Improved understanding of the causes of unwanted noise can lead to quieter designs. The sound radiated by these systems is generated by a number of mechanisms, which have been cataloged and described by many authors, including Blake [1], Wright [2] and Morfey [3]. The present work considered a simplified system consisting of a single rotor operating at a low Mach number such that the sound generated was predominantly dipole in nature, resulting from rigid blades interacting with a turbulent inflow.

The objective of the current paper is to present a new method for predicting the frequency-dependent magnitude of the dipole sound source created by a ducted rotor interacting with a casing turbulent boundary layer. This source of inflow noise is important, considering 1) a turbulent boundary layer is nearly always present in a ducted rotor system and may have much higher turbulence intensity than the bulk flow in the duct, 2) the relative speed of the rotor blades is highest at the tip, and 3) the many scales of turbulence in the boundary layer can lead to both tonal and broadband sound. An additional benefit of investigating this noise mechanism is that the turbulence is created without generating additional sound, as can be the case with turbulence grids or other devices.

One method for predicting rotor noise due to turbulence ingestion is to classify the turbulent motions as two separate sets based on spatial scales, and use separate methods for predicting each. A review paper by Huff [4] provides a number of examples. Using the criteria described by Blake [1], turbulence can be considered small scale if it passes through the rotor while interacting with only one blade, and considered large scale if it interacts with multiple blades. In the case of small-scale turbulence, the unsteady lift between any two rotor blades is statistically uncorrelated and is a source of broadband sound. For large-scale turbulence, the unsteady lift between consecutive blades is statistically correlated, which is a much more efficient mechanism for noise generation than uncorrelated lift. Deterministic inflow disturbances, such as stator wakes, can be treated as a special case of large-scale turbulence and are a source of tonal sound, because the rotor blades interact with the wakes at regular intervals. Hanson [5] studied turbulence ingestion noise with a rotor subjected to both periodic inflow disturbances and anisotropic turbulence with extremely long axial length. He identified sharp spectral peaks resulting from both inflows and concluded that narrowband turbulence caused coherent forces on the rotor in a manner that had previously been only attributed to fixed inflow distortion.

Compared with the literature that is focused on other fan noise sources, a relatively small number of studies have considered

boundary-layer interaction as a source of rotor noise. Moiseev et al. [6] studied a ducted rotor ingesting various casing boundary-layer inflows, including a natural boundary layer and an artificially thickened boundary layer. Correlation length scales of the various cases were measured in axial and tangential directions, and measurements of radiated sound spectra were presented for both a 10-bladed and a 17-bladed rotor. The use of a turbulence grid upstream of the rotor was found to reduce the tonal sound generated at multiples of blade passing frequency (BPF). The authors reported that this effect was likely due to breakup of large-scale axial motions. Increasing the thickness of the boundary layer was found to cause up to a 10 dB change in radiated sound for the 10-bladed rotor. Moiseev et al. conclude that most of the sound was generated at the hub and tip regions of the rotor and was due to the ingested boundary layers.

A study by Ganz et al. [7] used a suction system to remove the casing boundary layer upstream of a 20-blade fan, and examined the broadband sound radiated by the rotor with and without boundary-layer suction. It was found that, when the casing boundary layer was present, broad bumps in the sound spectra were observed centered about multiples of BPF and with magnitude of nearly 10 dB above the broadband level. These spectral features disappeared when the boundary-layer suction was applied. It was noted that the boundary layer was a significant source of sound, and it was concluded to be the source of the broad bumps found in the spectra.

The measurements presented by Ganz et al. [7] were studied by a number of authors, including the following studies focused on boundary-layer ingestion noise. Glegg and Walker [8] used a flat-plate cascade response function including blade spanwise effects to predict broadband noise due to a boundary-layer inflow. They developed a method to incorporate anisotropy into a wave number spectrum based on three turbulent length scales. They pointed out that "long thin eddies stretched in the direction of the flow are more likely to cause blade tones or spectral humps than isotropic eddies." This anisotropic wave number spectrum was used to produce acoustic predictions that agreed well with the measurements by Ganz et al. [7] when appropriate turbulent length scales were selected. Another cascade analysis was conducted by Joseph and Parry [9], who found that the turbulence length scales reported by Ganz et al. [7] were an order of magnitude too short to account for the broad humps at multiples of the blade passing frequency. Martinez [10] also developed an analytical model for broadband sound generated by a rotor ingesting anisotropic turbulence, and recognized that correlated sound between rotor blades led to broad humps in the spectra around blade-rate tones.

Atassi and Logue [11] used rapid distortion theory to develop a wave number spectra model that can account for anisotropic turbulence. A linear cascade model was used to relate the ingested turbulence to the acoustic response of the fan blades. Their model predicts broad humps at multiples of the blade rate that qualitatively agree with experiments when the turbulence is sufficiently stretched in the axial direction.

The present paper reports on a new method for predicting the noise generated by the interaction of a ducted rotor with a casing turbulent boundary layer. This method uses a gust upwash response function to relate the unsteady force on the rotor blades with the two-point correlation of upwash velocity. These upwash statistics experienced by the rotor blades are related to the two-point correlation statistics in the casing boundary layer in the space–time domain. These statistics explicitly take the inhomogeneous and nonisotropic character of boundary-layer flows into account. The interaction of a rotor with a casing boundary layer causes both correlated and uncorrelated upwash on the rotor blades, thus the sound prediction contains both tonal and broadband components. To validate this theory, a carefully designed experiment was developed to obtain acoustic measurements of a rotor ingesting a casing turbulent boundary layer. This experiment is described in the following section. An analytical representation of turbulence ingestion noise is then presented, along with a model for the relevant boundary-layer turbulence statistics. The rotor sound source prediction is compared with the measured sound source for two cases with different boundary-layer thicknesses. An additional case with radial inflow distortion was also tested, and reasonable agreement was found between prediction and experiment.

## II. Boundary-Layer Interaction Noise Experiment

An experimental facility was constructed as illustrated in Fig. 1. The duct was PVC with a machined inner diameter of 206 mm and a wall thickness of 6.7 mm. The system was supported by a vibration isolation pad and placed in an anechoic chamber with a low-frequency limit of 100 Hz. A number of design considerations were made to provide measurements of boundary-layer interaction noise while reducing other noise sources. A center cylinder with a 57 mm outside diameter extended upstream of the duct inlet to create an annular inflow passage and was cantilevered from supports located several duct diameters upstream of the inlet. This provided structural support for the rotor and motor without causing mean flow distortion. The inlet flow was conditioned using a single layer of a "cheesecloth-type" thin fabric with negligible acoustic impedance stretched over a cylindrical wire frame. A compact servo motor was housed in the center cylinder to direct drive the rotor at the desired speed, up to 5000 rpm (83 Hz). The rotor was a 10-bladed propeller previously used by Sevik [12], with tip diameter $D = 203.2$ mm and hub diameter of 50.8 mm, constant blade chord $C = 25.4$ mm, maximum thickness of 2.4 mm, and straight blades incorporating twist only. The rotor operated with a tip gap equal to 5% of the blade chord. The length of the duct was 1.4 m. The boundary-layer Reynolds number at the location of the rotor was varied by placing the rotor at different distances from the duct inlet, between $0 \leq L_1/D \leq 1.2$, where $L_1$ was measured from the termination of the inlet and the beginning of the straight casing.

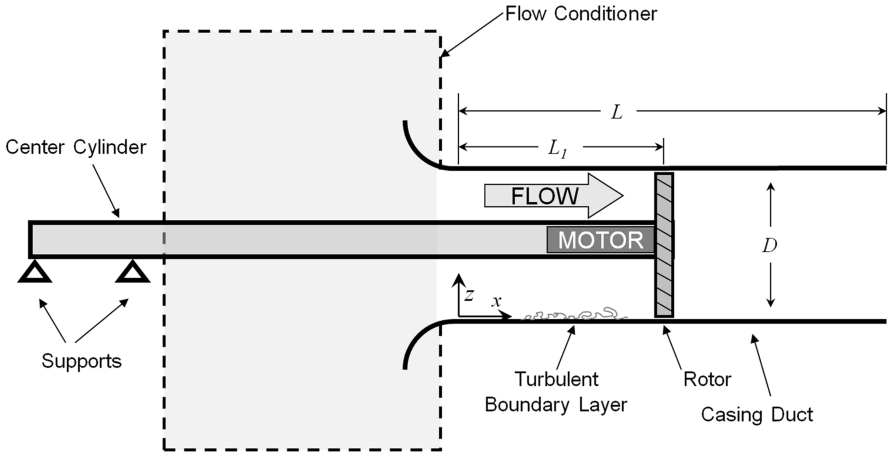


**Fig. 1 Schematic of ducted rotor model. Sketch not to scale.**

The laboratory reference frame was used to describe the measured boundary-layer quantities, as shown in Fig. 1. In this system, the origin is on the lower casing wall, $x$ is the axial direction, $z$ is the direction normal to the casing, and $y$ is used to describe the azimuthal direction. This coordinate system was chosen as typical of boundary-layer studies. Note that the ratio of the boundary-layer thickness to the surface curvature was less than 0.1 for the inlet flow considered here. Measurements of the boundary-layer statistics presented later in this paper demonstrate that the casing boundary layer is essentially similar to a flat-plate boundary layer.

### A. Interaction Noise Isolation

The best possible experimental estimate for the sound created by the rotor ingesting a turbulent boundary layer was found by documenting and subtracting the rotor self-noise from the total sound spectrum. The term "self-noise" refers to sound produced by the rotor in the absence of inflow turbulence. A number of mechanisms contribute to the total self-noise generated by the rotor, such as trailing-edge noise, tip leakage effects, as well as Gutin noise at higher Mach numbers. The radiated self-noise was measured by placing the rotor at an axial position of $L_1/D = 0.125$ such that the inflow boundary layer was minimized and the rotor was exposed to an inflow that was essentially steady and axisymmetric. This axial location was found to be a minimum for radiated sound. The radiated sound was then obtained as a function of rotor flow coefficient, defined as $\phi = \bar{U}/V_{\text{tip}}$, where $\bar{U}$ is the spatial average of the axial velocity in the duct and $V_{\text{tip}}$ is the rotor tip velocity. The flow rate through the duct was decreased independently from rotor speed by applying a variable restriction in the form of thin fabric with negligible effect on the acoustic field to the duct exit. The duct flow rate was increased by attaching the outlet of the duct to an acoustically treated chamber connected to a centrifugal fan, with baffles to block line of sight between the centrifugal fan and the duct of interest. A variable speed drive on the centrifugal fan provided a way to precisely set the flow rate through the duct. The centrifugal fan was operated at less than 10% of rated speed, and was an insignificant source of noise for the current experiment. Microphone measurements were acquired at 11 rotor speeds between 2500 and 5000 rpm, and at the flow coefficients of $0.15 \leq \phi \leq 0.43$, in increments of 0.01. A single microphone was located at a distance of 1.85 m from the duct inlet and 9.5 deg off axis. The pressure rise developed by the rotor $\Delta p$ was nondimensionalized as $\psi = 2\Delta p/\rho V_{\text{tip}}^2$. The dependence of $\psi$ on $\phi$, as well as the dependence of the radiated sound pressure level (SPL) on $\phi$, are shown in Fig. 2. It can be seen that the rotor self-noise was minimized for $\phi = 0.39$. The remainder of the measurements presented in this paper were acquired at this operating condition, corresponding to very lightly loaded rotor blades, with $\psi$ slightly nonzero.

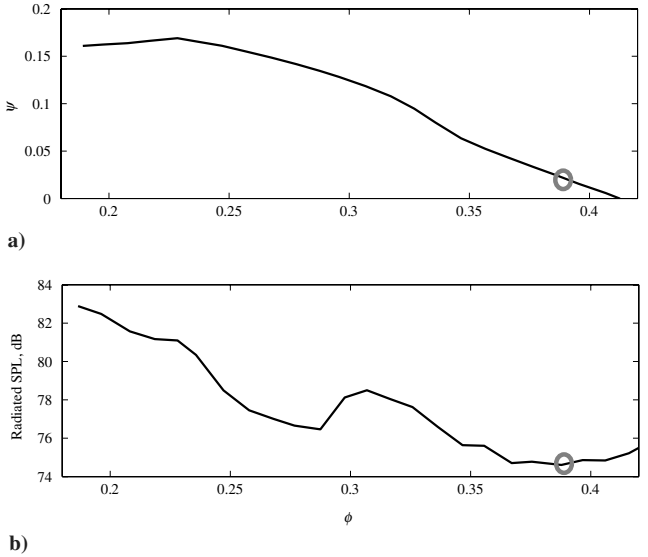


**Fig. 2 Dependence of a) $\psi$ on $\phi$, and b) radiated SPL on $\phi$. Circle indicates operating condition where rotor self-noise was found to be minimized.**

The radiated sound from the ducted rotor system was then measured as a function of the rotor axial location $L_1/D$ while the flow rate was maintained at $\phi = 0.39$. The cantilevered center cylinder with attached servo motor and rotor allowed for positioning the rotor at a range of axial positions within the duct. Radiated sound spectral densities are shown in Fig. 3, referenced to 20 $\mu$Pa. The sound was found to increase with rotor axial location across all frequencies between approximately 1000 and 8000 Hz. The sound generated at $\phi = 0.39$ (the quietest flow rate) and $L_1/D = 0.125$ (the quietest axial location) was found to be a minimum, and was defined as the self-noise generated by the rotor. These spectra were subtracted from the spectral measurements obtained with the rotor placed at other $L_1$ locations. The turbulent boundary-layer ingestion noise was found to increase by approximately 1 dB per 0.125 $L_1/D$, so that the self-noise subtraction represents relatively minor correction for values of $L_1/D > 0.5$. It was assumed that the self-noise was unchanged when the rotor was subjected to a casing turbulent boundary layer. This procedure was found to provide the best possible estimate of the radiated sound caused by the interaction of the rotor blades with the casing boundary layer.

### B. Net Sound Source Identification

The fan noise spectra measured in the far field includes the effects of the acoustic transfer function between the distributed sound sources and the observer location. This transfer function is complicated by the location of the sound sources within a rigid duct. For example, many of the spectral features observed in Fig. 3 are related to the "organ pipe" resonances of the duct. These effects were accounted for by using a decomposition algorithm described in [13], which identifies an acoustic transfer function from a set of radiated sound spectral density measurements acquired at a range of rotor tip speeds. The result of this processing method is a function, denoted $|\chi|^2$, that represents the net acoustic transfer function effect of the duct. The net frequency-dependent unsteady thrust of the rotor $\mathcal{F}$ is related to the radiated sound pressure spectral density by

$$\Phi_{p_{\text{rad}}} = \mathcal{F}|\chi|^2 g_{\text{fs}}^2 k^2 \cos^2\alpha \tag{1}$$

where $g_{\text{fs}}$ is the free-space Green's function and is multiplied by the acoustic wave number $k$ and $\cos\alpha$ to give the dipole transfer function; where $\alpha$ is the angle between the axis of the dipole and the observer. This equation simply represents the radiated sound of the rotor as an unsteady force spectra multiplied by the free-space dipole radiation pattern and by the function $|\chi|^2$. Note that $|\chi|^2$ is dependent

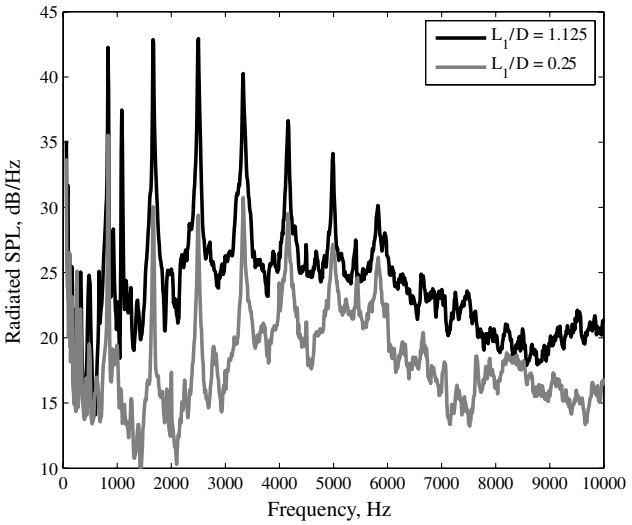


**Fig. 3 Radiated sound as a function of rotor axial location $L_1/D$. Rotor shaft rate = 67 Hz.**

on the geometry of the system, including the length of the duct, the rotor location within the duct, and the observer location. In the present experiment, the most significant spectral features in $|\chi|^2$ are organ pipe modes with magnitude of $\approx$10 dB. These effects and plots of $|\chi|^2$ are considered in more detail in [13].

As discussed in [13], if near-field transfer function effects are not significant, then $\mathcal{F}$ approximately equals the autospectral density of the net unsteady force on the rotor. An analytical representation of this same function will be derived in the next section, denoted $[\Phi_{FF}(\omega)]_{\text{rotor}}$. At low frequencies, where only plane waves propagate in the duct (less than 1 kHz for the present dimensions), the $\mathcal{F}$ obtained from experimental measurements should be identical to the true $[\Phi_{FF}(\omega)]_{\text{rotor}}$. Near-field effects could lead to additional features in the radiated sound. For example, when the rotor blade spacing is not acoustically compact, the coupling between the correlated blade forces and the higher order acoustic duct modes could lead to a change in the net radiation efficiency. However, the sound radiated by the finite length duct under consideration does not exhibit significant spectral features at the expected cut-on frequencies of higher-order duct modes. The major spectral features found in Fig. 3 are blade-rate tones and organ pipe modes. Gliebe [14] also noted little duct cut-on behavior, and suggested the stochastic nature of noise due to turbulence did not create well-defined modal behavior. The present work will assume $\mathcal{F} \approx [\Phi_{FF}(\omega)]_{\text{rotor}}$ for the purpose of comparing the theoretical prediction with the experiments.

The unsteady force spectral density can be nondimensionalized by the rotor diameter $2r_{\text{tip}}$, fluid approach velocity at the rotor tip $U_{\text{tip}}$, and the dynamic pressure based on blade tip velocity $\rho U_{\text{tip}}^2/2$ to define

$$\mathcal{F}^* = \frac{\mathcal{F}}{8\rho^2 U_{\text{tip}}^3 r_{\text{tip}}^5} \tag{2}$$

The function $\mathcal{F}^*$ is shown in Fig. 4 for the same rotor axial locations as shown in Fig. 3. Many of the spectral features observed in Fig. 3 were quantified as the functions $|\chi|^2$, which were calculated for each $L_1/D$ location, and have been removed. The result is a significantly more tractable representation of the rotor noise. Note that significant broadband and tonal features are observed in the spectra. Note also that these data represent only turbulent boundary-layer interaction noise, where the time-average statistics of the approach flow are axisymmetric. The relatively large amplitude tones observed will be shown to be related to the turbulent structure of the boundary layer, and are not a result of circumferential variation in the mean flow velocity.

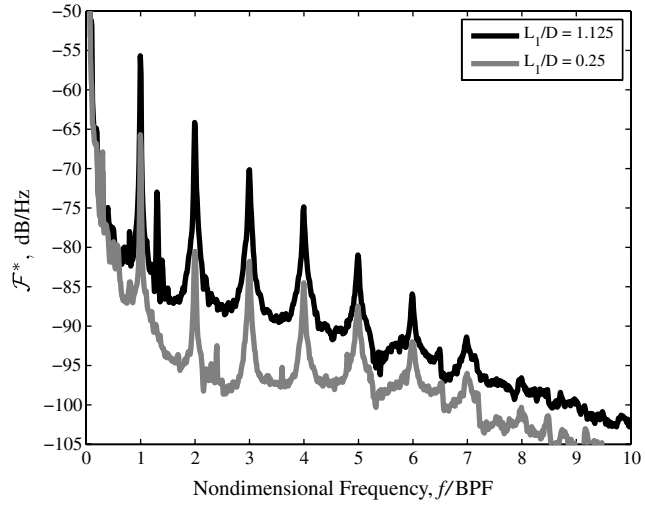


**Fig. 4 Sound source measurement as a function of rotor axial location $L_1/D$. Rotor shaft rate = 67 Hz.**

## III. Analytical Model for Net Unsteady Lift

An analytical representation of the net unsteady thrust experienced by the rotor can be derived by beginning with the unsteady lift force $F$ on an airfoil in terms of a gust response function $\mathcal{L}$,

$$\frac{\mathrm{d}F(\omega)}{\mathrm{d}s} = \pi\rho C U(s)\mathcal{L}(\omega)\hat{w}(s,\omega) \tag{3}$$

where this equation is in the airfoil coordinate system, with streamwise, spanwise (denoted $s$), and transverse directions, as noted in Fig. 5. In this equation, $C$ is the airfoil chord, $\rho$ is the fluid density, $U$ is the fluid approach velocity as a function of blade airfoil span, and $\hat{w}$ is the Fourier representation of the transverse gust. The rotor in the present experiment has blades with constant chord. Integrating both sides with respect to span gives the lift on a finite airfoil,

$$F(\omega) = \int \pi\rho C U(s)\mathcal{L}(\omega)\hat{w}(s,\omega)\,\mathrm{d}s$$

The analysis is simplified by considering the term $U$ to be a constant. The relative fluid approach velocity to the rotor is a linear function of the radial location on the blade. In the case that the rotor is ingesting boundary-layer turbulence only, however, $\hat{w}$ is zero for most of the blade span, and the term $U$ is nearly constant over the small portion of the span where the rotor blades interact with the casing boundary layer. This would also be a reasonable assumption in the case of a rotor with a hub-to-tip ratio close to one. In the case $U$ is approximately constant, Eq. (3) can be given as

$$F(\omega) = \pi\rho C U\mathcal{L}(\omega)\int \hat{w}(s,\omega)\,\mathrm{d}s \tag{4}$$

The total unsteady force on a rotor with $B$ blades is found by adding the lift contribution from each blade. For simplicity of notation, let $\beta(\omega) = \pi\rho C U\mathcal{L}(\omega)$. The index $n$ is used to indicate the blades numbered from one to $B$, giving

$$[F(\omega)]_{\text{rotor}} = \beta(\omega)\sum_{n=1}^{B}\int \hat{w}(s_n,\omega)\,\mathrm{d}s_n \tag{5}$$

The definition of the spectral density function in terms of the Fourier transform of a stationary random process is given by Bendat and Piersol [15]. The spectral density of unsteady thrust can be represented as

$$[\Phi_{FF}(\omega)]_{\text{rotor}} = \lim_{T_0\to\infty} E\left[\frac{1}{T_0}[F(\omega)]_{\text{rotor}}[F^*(\omega)]_{\text{rotor}}\right]$$

or

$$[\Phi_{FF}(\omega)]_{\text{rotor}} = \beta^2(\omega)\lim_{T_0\to\infty} E\left[\frac{1}{T_0}\sum_{n=1}^{B}\int \hat{w}(s_n,\omega)\,\mathrm{d}s_n\sum_{m=1}^{B}\int \hat{w}^*(s'_m,\omega)\,\mathrm{d}s'_m\right] \tag{6}$$

where the $*$ denotes the complex conjugate. The variable $m$ is the second blade numbering index, and $s'$ is the rotor blade span location on the $m$-numbered blades. Equation (6) can be rearranged, giving

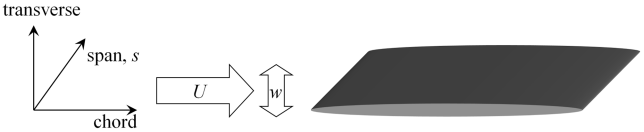


**Fig. 5 Coordinate system and velocity definitions for airfoil gust equation.**

$$[\Phi_{FF}(\omega)]_{\text{rotor}} = \beta^2(\omega)\sum_{n=1}^{B}\sum_{m=1}^{B}\iint \lim_{T_0\to\infty} E\left[\frac{1}{T_0}\hat{w}(s_n,\omega)\hat{w}^*(s'_m,\omega)\right] \mathrm{d}s'_m\,\mathrm{d}s_n \quad (7)$$

The integrand is the cross-spectral density of the upwash velocity fluctuations as observed by the rotor blades, and so Eq. (7) can be equivalently expressed as

$$[\Phi_{FF}(\omega)]_{\text{rotor}} = \beta^2(\omega)\sum_{n=1}^{B}\sum_{m=1}^{B}\iint \Phi_{ww}(s_n, s'_m, \omega)\,\mathrm{d}s'_m\,\mathrm{d}s_n \quad (8)$$

This equation could be evaluated using one of a variety of turbulent spectra models to approximate $\Phi_{ww}$ in the frequency–wave-number domain. Analytical representations such as the von Kármán spectra could be substituted to approximate homogeneous and isotropic turbulence. An example simplification for homogeneous and isotropic turbulence ingestion noise is presented in the Appendix and is readily compared to previously published solutions. However, it will be shown to be a significant advantage to model the effects of anisotropic, nonhomogeneous turbulence in the space–time domain, rather than using a frequency–wave-number representation. The definition of the spectral density function in terms of the cross-correlation function is

$$\Phi_{ww}(s_n, s'_m, \omega) = \int_{-\infty}^{\infty} R_{ww}(\tau, s_n, s'_m)e^{-i\omega\tau}\,\mathrm{d}\tau$$

which can be substituted into Eq. (8) to give

$$[\Phi_{FF}(\omega)]_{\text{rotor}} = \beta^2(\omega)\int_{-\infty}^{\infty}\left[\sum_{n=1}^{B}\sum_{m=1}^{B}\iint R_{ww}(\tau, s_n, s'_m)\,\mathrm{d}s'_m\,\mathrm{d}s_n\right]e^{-i\omega\tau}\,\mathrm{d}\tau \quad (9)$$

after the order of integration operators has been rearranged. This equation is valid for any turbulent field that can be represented as $R_{ww}$. This model is an advancement over previous studies in that it can include the effects of inhomogeneous and nonisotropic turbulence, arbitrary blade spacing, any number of rotor blades, and asymmetric inflow turbulence. The function $R_{ww}(\tau, s_n, s'_m)$ represents the two-point correlation of upwash velocity on the rotor blades. In the case of azimuthally homogenous turbulence and equally spaced rotor blades, such as in the present experiment, the function $R_{ww}(\tau, s_n, s'_m)$ is dependent on only the difference $m - n$. In this case, let $m = 1$ and replace the summation over $m$ with multiplication by the number of blades $B$ to get

$$[\Phi_{FF}(\omega)]_{\text{rotor}} = B\beta^2(\omega)\int_{-\infty}^{\infty}\left[\sum_{n=1}^{B}\iint R_{ww}(\tau, s_n, s'_1)\,\mathrm{d}s'_1\,\mathrm{d}s_n\right]e^{-i\omega\tau}\,\mathrm{d}\tau \quad (10)$$

The analytical predictions presented later in this paper were found by evaluating this expression. The next section provides detailed measurements and a model of the two-point statistics of the boundary layer that are required for the evaluation of Eq. (10).

## IV. Characterization of Casing Boundary Layer

Equation (10) relates the rotor noise to the two-point correlation of upwash velocity $R_{ww}(\tau, s_n, s'_m)$ as observed by the rotor blades. To evaluate this expression, some measurement or analytical model of $R_{ww}(\tau, s_n, s'_m)$ must be used. In lieu of measurements in the blade reference frame, which would require the use of multiple sets of rotating velocity probes, measurements were made of the function $R_{uu}(\tau, \Delta y, z, z_{\text{ref}})$ in the laboratory frame. The four independent variables represent the time delay or lag $\tau$, the spacing in the circumferential ($\Delta y = r\Delta\theta$) direction, the wall-normal direction $z$, and the wall-normal position of the reference location $z_{\text{ref}}$. The rotor blade spanwise direction $s$ is identical to the casing boundary-layer wall-normal direction $z$, and variable $s'$ will be denoted $z_{\text{ref}}$ when referred to as a boundary-layer location. The correlation function, as observed in the blade reference frame $R_{ww}(\tau, s_n, s'_m)$, is identical to the function $R_{uu}(\tau, \Delta y, z, z_{\text{ref}})$ for the path in $\tau$ and $\Delta y$ described by the blade motion, if the unsteady axial velocity $\tilde{u}$ in the casing reference frame can be treated as the unsteady upwash velocity in the rotor blade reference frame. This is reasonable as long as the stagger angle of the rotor blades is high, and allows single component velocity measurements made in the laboratory reference frame to suffice for measuring the upwash in the rotating frame. It was also assumed that the approach turbulence is not distorted by the rotor. These assumptions are typical of many turbulence ingestion noise studies. The relationship between $R_{ww}(\tau, s_n, s'_m)$ and $R_{uu}(\tau, \Delta y, z, z_{\text{ref}})$ is an important part of the evaluation of Eq. (10) and will be illustrated in Sec. V.

Experimental measurements of the velocity statistics in the approach flow to the rotor were made with the intent to describe $R_{uu}(\tau, \Delta y, z, z_{\text{ref}})$. Measurement of this entire function was beyond the scope of the present work and, to the knowledge of the present authors, only small subsets of this function have been measured previously in turbulent boundary-layer flows. The approach taken in this paper was to document a subset of this function and to use a simple model to estimate the complete four-dimensional correlation function.

The ducted rotor system was removed from the anechoic chamber to facilitate the measurement of the approach flow to the rotor. The rotor was removed from the center cylinder, such that hot-wire probes could then be placed at the streamwise location corresponding to the leading edge of the rotor during the acoustic experiments. The hot-wire probes were positioned on a traverse with radial and azimuthal movement. The duct inlet was connected to a large pressurized plenum that was adapted from a wind tunnel, and the same flow conditioner was used. The flow rate corresponding to a rotor speed of 4000 rpm and $\phi = 0.39$ was established by the auxiliary blower acting on the plenum. The two-point correlation function was surveyed in two planes, one (radial) with zero probe separation in the circumferential direction ($\Delta y = 0$) and one (azimuthal) with the probes at the same wall-normal location ($z = z_{\text{ref}}$).

These measurements were used to create an empirical model for the two-point correlation function of axial velocity in the casing boundary layer. The model was based on the autocorrelation of axial velocity with an exponential decay in the cross-stream directions. The remainder of this section will describe the details of the measurement and the model.

### A. Single Point Velocity Statistics

The momentum thickness of the casing boundary layer was measured as a function of the streamwise location $L_1/D$ and ranged from $\theta = 0.34$ mm at $L_1/D = 0.125$ to $\theta = 0.82$ mm at $L_1/D = 1.125$. The remaining boundary-layer measurements presented in this paper were made at $L_1/D = 1.125$ only, and were nondimensionalized by $\theta$ and $\bar{U}$. The location $L_1/D = 0.125$ corresponds to the best location for measurement of both the acoustics and turbulence. It was the furthest into the duct the rotor could be safely cantilevered and, as such, was the documented case where the boundary layer was the thickest. For this reason, the inflow noise was the loudest and boundary-layer statistics were easiest to measure. For reference, the displacement thickness at this location was found to be $\delta^* = 1.02$ mm with a corresponding boundary-layer thickness of $\delta_{99} = 11$ mm. The variance as a function of $z_{\text{ref}}$ is shown in Fig. 6. It can be noted that this function is essentially zero for $z_{\text{ref}}/\theta > 14$, or about 1 cm from the duct wall. This justifies the assumption of constant velocity made in Eq. (4). For reference, the center of the rotor hub is at approximately $130\theta$. A least-square method was used to fit a polynomial to the variance, indicated in Fig. 6. The equation for this polynomial was found to be

$$\frac{\overline{\tilde{u}^2}(z_{\text{ref}}/\theta)}{\bar{U}^2} = -3.1\times10^{-5}\left(\frac{z_{\text{ref}}}{\theta}\right)^2 - 1.0\times10^{-3}\left(\frac{z_{\text{ref}}}{\theta}\right) + 8.6\times10^{-3} \quad (11)$$

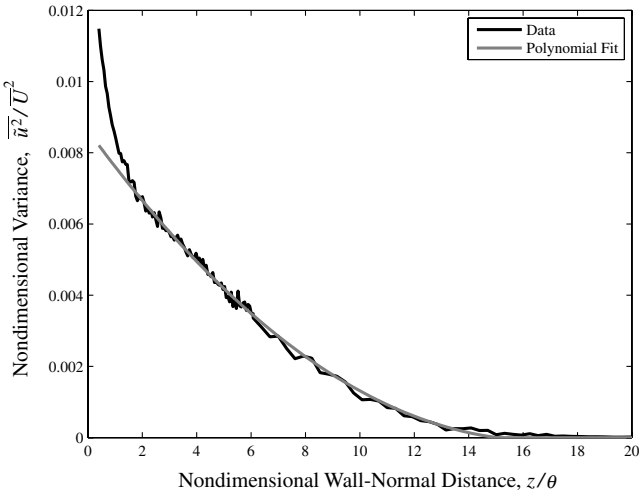


**Fig. 6 Variance of axial velocity in duct boundary layer, measured at $L_1/D = 1.125$. Polynomial fit is given in Eq. (11); $\theta = 0.82$ mm. For reference, the center of the duct is at $130\theta$.**

The fit provides an accurate representation of the data for $1 < z_{\text{ref}}/\theta < 14$. Values of $z_{\text{ref}}/\theta < 1$ are not used in the present calculation, because the tip of the rotor is at approximately $1.5\theta$.

Autocorrelation functions measured at $L_1/D = 1.125$ are shown varying with wall-normal distance in Fig. 7 for $\tau\bar{U}/\theta > 0$. This figure shows the autocorrelations in a log-linear format, normalized by the variance, with the notation

$$R^*_{uu}(\tau, z_{\text{ref}}) = \frac{R_{uu}(\tau, z_{\text{ref}})}{\overline{\tilde{u}^2}(z_{\text{ref}})} \tag{12}$$

The function $R^*_{uu}(\tau, z_{\text{ref}})$ is observed to have a complicated shape, combining a low-frequency, large-scale decay at large values of $\tau$ and a small-scale paraboliclike shape when $\tau\bar{U}/\theta < 10$. When $\tau\bar{U}/\theta > 10$, there is considerable dependence on the wall-normal distance. This is reasonable to expect because the small scales of turbulence are largely insensitive to the wall location, whereas few large scales will be present near the wall and more will be expected near the freestream. Autocorrelation functions at the three values of $z_{\text{ref}}/\theta$ shown in Fig. 7 were selected as representative of the different shapes found in the boundary layer. Seventh-order polynomials were found to fit the log-linear plot satisfactorily, and the coefficients of these functions are given in Table 1. The data were fit using the range $|\tau\bar{U}/\theta| < 4000$. Note that the curve fit used $\ell_n\,|\tau\bar{U}/\theta|$ as the independent variable. This caused the polynomial to emphasize the long scales and match them best. Finally, the polynomial fits were found to deviate from the data for values of $\tau\bar{U}/\theta$ near zero. To correct this behavior, values of $|\tau\bar{U}/\theta| < 1$ were replaced with spline interpolation, resulting in a smooth parabolic fit near $\tau = 0$. Linear interpolation was used for values of $z_{\text{ref}}/\theta$ between the three curves selected. The result of this modeling is that, for a given value of $z_{\text{ref}}$, the normalized autocorrelation $R^*_{uu}(\tau, z_{\text{ref}})$ as a function of $\tau\bar{U}/\theta$ can be calculated, and the magnitude of the variance can be found from Eq. (11). Autocorrelation functions obtained in this way were found to agree quite well with measurements from all values of $z_{\text{ref}}$ at $L_1/D = 1.125$.

### B. Two-Point Correlation of Axial Velocity

Measurements of the two-point cross correlation of axial velocity were made in two orthogonal planes. A plane in the azimuthal direction was surveyed, with both probes held at $z_{\text{ref}} = 4$ mm, while an azimuthal traverse moved one probe away from the other in the $y$ direction. Because the boundary layer is homogeneous in this direction, absolute $y$ locations are not important, and the measurement was denoted in terms of $\Delta y$. A wall-normal plane was also surveyed with $z_{\text{ref}} = 1.3$. The time-series measurements were high-pass filtered at 2 Hz to remove the effect of a spatially uniform unsteadiness in the streamwise velocity in the duct. Results are shown as the upper plots in Figs. 8 and 9. The correlation contours are seen to have a complicated shape, with large streamwise extent and small extent in the streamwise-normal directions.

The polynomial fit for the autocorrelation function described in the previous section represents the two-point correlation function for $\Delta y = z - z_{\text{ref}} = 0$. The cross correlation for spatially separated points was accounted for using an exponential decay from the autocorrelation in the cross-stream directions. Specifically, the cross correlation was modeled as an exponential decay based on a dimensionless length $r^*_{yz}$ in the $y$-$z$ plane, defined as

$$r^*_{yz} = \left[\left(\alpha_y \frac{\Delta y}{z_{\text{ref}}}\right)^2 + \left(\alpha_z \frac{z - z_{\text{ref}}}{z_{\text{ref}}}\right)^2\right]^{\frac{1}{2}} \tag{13}$$

where $\alpha_y$ and $\alpha_z$ are constants. The four-dimensional model used to approximate the two-point correlation of axial velocity is given as

$$R_{uu}(\tau, \Delta y, z, z_{\text{ref}}) = R_{uu}(z_{\text{ref}}, \tau) e^{[-R^*_{uu}(z_{\text{ref}}, \tau) r^{*2}_{yz}]} \tag{14}$$

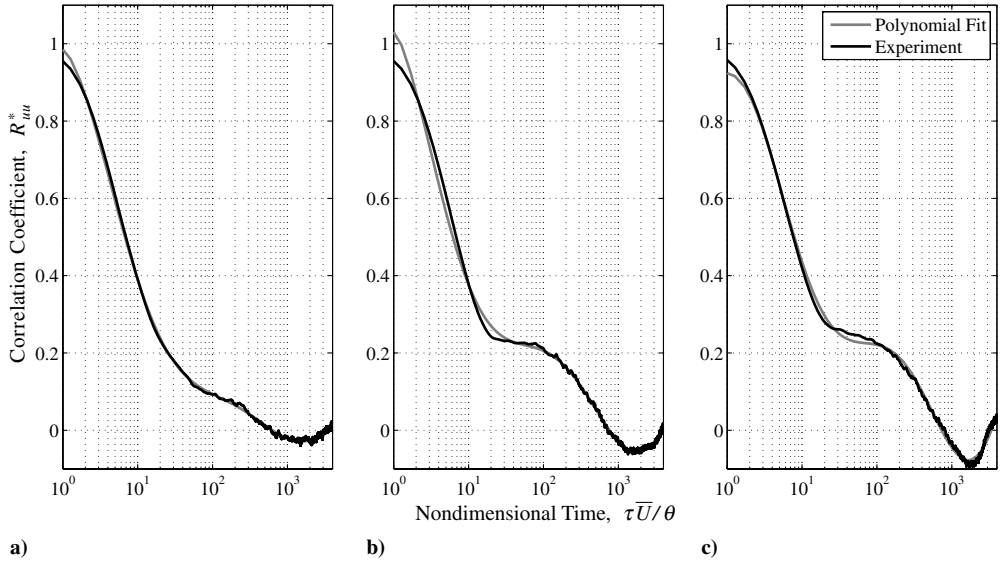


**Fig. 7 Measured autocorrelation functions $R^*_{uu}(\tau\bar{U}/\theta)$ along with polynomial fits, illustrating the difference in shape between the near-wall region and the outer boundary-layer region. Measurement location: $L_1/D = 1.125$; a) $z_{\text{ref}}/\theta = 1.57$, b) $z_{\text{ref}}/\theta = 5.89$, c) $z_{\text{ref}}/\theta = 7.92$.**

**Table 1 Polynomial coefficients used in modeling nondimensional autocorrelation $R^*(\tau\bar{U}/\theta, z_{\text{ref}})$**

| | $z_{\text{ref}} = 1.57$ | $z_{\text{ref}} = 5.89$ | $z_{\text{ref}} = 7.92$ |
|---|---|---|---|
| $[\ell_n(\tau\bar{U}/\theta)]^7$ | −1.7321e-005 | −4.4462e-005 | −1.8251e-005 |
| $[\ell_n(\tau\bar{U}/\theta)]^6$ | 4.7418e-004 | 1.2829e-003 | 4.4601e-004 |
| $[\ell_n(\tau\bar{U}/\theta)]^5$ | −4.5661e-003 | −1.3639e-002 | −3.3148e-003 |
| $[\ell_n(\tau\bar{U}/\theta)]^4$ | 1.5828e-002 | 6.3215e-002 | 1.9623e-003 |
| $[\ell_n(\tau\bar{U}/\theta)]^3$ | 1.0446e-002 | −1.0328e-001 | 6.9082e-002 |
| $[\ell_n(\tau\bar{U}/\theta)]^2$ | −1.3729e-001 | −4.5695e-002 | −2.1106e-001 |
| $[\ell_n(\tau\bar{U}/\theta)]^1$ | −9.3164e-002 | −2.4849e-002 | −1.2436e-001 |
| const | 9.9060e-001 | 9.2583e-001 | $1.0382e+000$ |

where the exponential scaling is multiplied by the dimensionless autocorrelation at the corresponding value of $\tau$. This results in an exponential decay in the spatial separation distance that is proportional to the magnitude of the autocorrelation. That is, it falls off faster when the autocorrelation is high, and slower when the autocorrelation is low. This behavior was found to agree well with the experimental measurements. Values for $\alpha_y$ and $\alpha_z$ were determined by evaluating the model at each of the data points used in the $\tau$-$y$ and $\tau$-$z$ hot-wire experiment. An error was calculated by taking the mean of the squared difference between the model and the experimental data. This error was a minimum for values of $\alpha_y = 1.68$ and $\alpha_z = 2.26$. Because the planes surveyed were at $z - z_{\text{ref}} = 0$ and $\Delta y = 0$, each parameter was determined independently. Results are shown in the lower plots of Figs. 8 and 9. It can be seen that the model represents the spatial and temporal extent of the measured correlation contours fairly well.

### C. Boundary-Layer Turbulence Discussion

A number of previous studies have focused on measurements of two-point velocity statistics in canonical boundary layers. Although the present paper is focused on turbomachinery noise, a brief review of these previous studies is extremely relevant. The space–time correlation contours shown are qualitatively similar to previous studies, although differences in the boundary layer (momentum thickness, displacement thickness, Reynolds number) and measurement locations $z_{\text{ref}}$ make quantitative comparisons more difficult. Kovasznay et al. [16] used hot-wire probes to study the spatial extent of what they called the large-scale or lasting features of a turbulent boundary layer. They were one of the first to comment on the streamwise elongation of the correlation surfaces. As a point of particular interest to the present study, they explain their extensive use of the space–time domain for representing turbulent flows by noting that "it was felt that the important and rather striking spatial relationships become obscured by spectral representation." More recent studies by both Ganapathisubramani et al. [17] using particle image velocimetry and by Krogstad and Antonia [18] using $x$-wire probes also found streamwise-elongated correlation contours of similar temporal and spatial extent to the present measurements.

Important observations on boundary-layer turbulence have also been made by Zhou et al. [19], who examined results from a direct numerical simulation study of channel flow. They note the presence of so-called hairpin vortices and found that these structures dissipate very gradually, over approximately 500 viscous time units, and can travel over 10,000 viscous wall units. In the present experiment, 10,000 viscous wall units corresponds to around $20\delta$, which is long enough to interact with many rotor blades. These hairpin vortices generate what Adrian et al. [20] call "packets" of induced low-speed fluid, which are produced near the wall and are elongated as they move toward the freestream and encounter higher speed fluid. Hutchins and Marusic [21] used a spanwise ($y$ in the current notation) rake of 10 hot-wire probes to better document the streamwise extent of the structures in the outer part of the log region. They found that these structures meander in the spanwise direction, and thus their true length is unmeasurable with a single probe because the structure may move in and out of the measurement volume. Coherent streaks of low-momentum fluid were observed to exist with length scales on the order of 10–$20\delta$. These elongated low-speed streaks are likely the source of the axially elongated correlation regions measured in the present study. The meandering of these structures leads to the width of the correlation contours and likewise provides an explanation for the spectral width of the blade-rate tones found in the acoustic measurements.

## V. Acoustic Prediction Results

A model for the full, four-dimensional, two-point correlation of axial velocity in a boundary layer has been presented as Eq. (14). This allows for the evaluation of Eq. (10) to predict the sound source. The two-point correlation experienced by the rotor $[R_{ww}(\tau, s_n, s'_m)]$ is a subset of the two-point correlation function in the boundary layer $[R_{uu}(\tau, \Delta y, z, z_{\text{ref}})]$. Specifically, the rotor blades cut a path in time and space through the boundary-layer correlation function. For

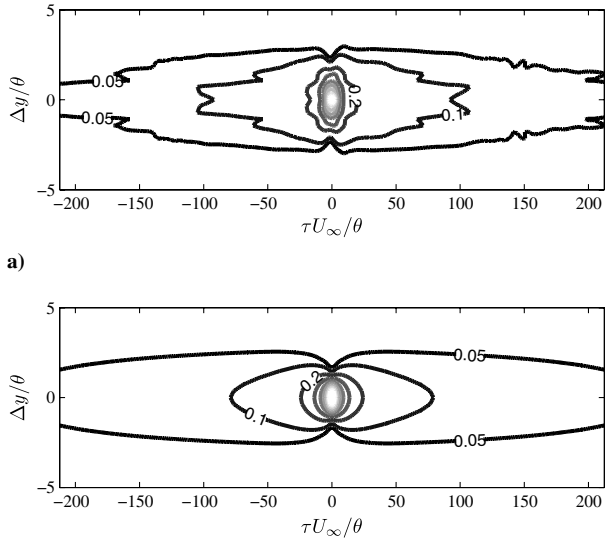


**Fig. 8 Comparison of axial velocity cross-correlation measurements with model in $\Delta y/\theta$ and $\tau\bar{U}/\theta$ plane. Contour levels are of velocity correlation coefficient at 0.05, 0.1, and higher, in increments of 0.1; $z_{\text{ref}}/\theta = 1.58$: a) experiment, b) model.**

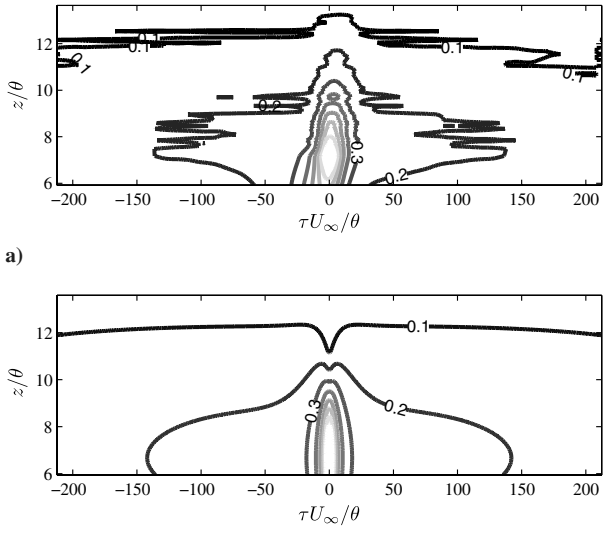


**Fig. 9 Comparison of axial velocity cross-correlation measurements with model in $z/\theta$ and $\tau\bar{U}/\theta$ plane. Contour levels are of velocity correlation coefficient in increments of 0.1; $z_{\text{ref}}/\theta = 6.67$: a) experiment, b) model.**

illustration purposes, a qualitative sketch of successive rotor blade paths through a fictitious boundary-layer cross-correlation function is given as Fig. 10. The rotor blades are $2\pi r_{\text{tip}}/B$ apart in the spanwise direction $\Delta y$ in the casing boundary layer, also defined as the pitch. The rotor blade path through the boundary-layer correlation contours is given by $\Delta y = \tau V_{\text{tip}}$, and $V_{\text{tip}}$ is thus the slope of the lines in Fig. 10. Given values of $\tau$ and $\Delta y$, along with blade span locations $z$ and $z_{\text{ref}}$, the boundary-layer two-point correlation from the perspective of the rotor blades can be found using Eq. (14). The value of the example correlation coefficient experienced by the rotor blades is shown in Fig. 11 for $z = z_{\text{ref}}$. Once the function $R_{ww}(\tau, s_n, s'_m)$ has been evaluated for all values of $s$, $s'$, and for all blades $n$, then Eq. (10) can be evaluated. The function $R_{ww}(\tau, s_n, s'_m)$ is double integrated over the blade span, then summed over $B$. The result is that the term in brackets in Eq. (10) has a maxima at each integer value of $\tau$BPF, at least for the present study. Note that, if the correlation function decays slowly enough in $\tau$, the unsteady lift on a given rotor blade may be correlated with itself after completing an entire rotation, in addition to being correlated with the other blades.

The acoustic predictions that follow used the unsteady gust response function $\mathcal{L}$ derived by Amiet, with the second-order solution [22] used at low frequencies ($[M\pi fC]/[(1-M^2)U_{\text{tip}}] < \pi/4$) and the high-frequency solution [23] used for ($[M\pi fC]/[(1-M^2)U_{\text{tip}}] > \pi/4$). For the low blade tip Mach numbers considered in the present experiment, the Amiet response function is not meaningfully different than the usual approximation for the Sears function given by Liepmann [24]. Additionally, the thickness correction suggested by Howe [25] was used, where $h$ is the blade thickness. The combined approximation for the response function was then

$$\mathcal{L}(\omega) = \frac{e^{-(\omega h/2U_{\text{tip}})}}{1 + (\pi\omega C/U_{\text{tip}})} \tag{15}$$

The current experiment used a low solidity fan with nonoverlapping blades. In the case of a rotor with overlapping blades, the use of a cascade response function would be important. Cascade response functions have been discussed by Glegg [26] and Atassi et al. [27], among others.

The results presented used spanwise integrations (over $s$ and $s'$ on the rotor blades) carried out over five locations between the rotor tip and $z_{\text{ref}}/\theta = 14$, where the velocity variance essentially becomes zero. The sample frequency of points in $\tau$ used to evaluate the model was 150 kHz. The calculation was carried out over $-1600 \le \tau\bar{U}/\theta \le 1600$. These values were found to be adequate to provide a converged solution.

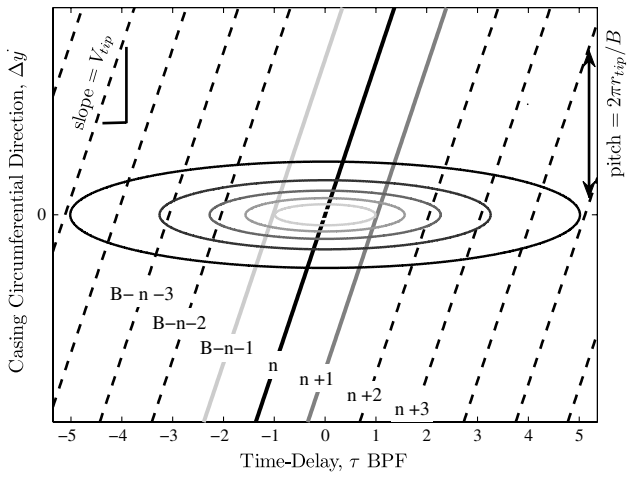


**Fig. 10 Sketch of rotor path through boundary-layer correlation contours. Dotted lines indicate rotor blade path.**

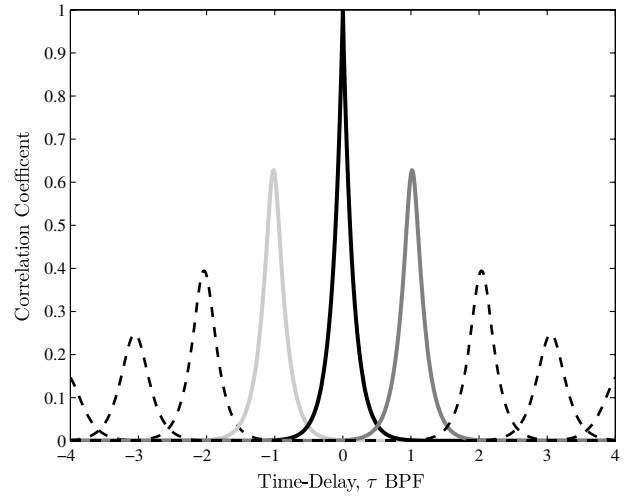


**Fig. 11 Correlation coefficient experienced by rotor blades as a function of time delay and blade number.**

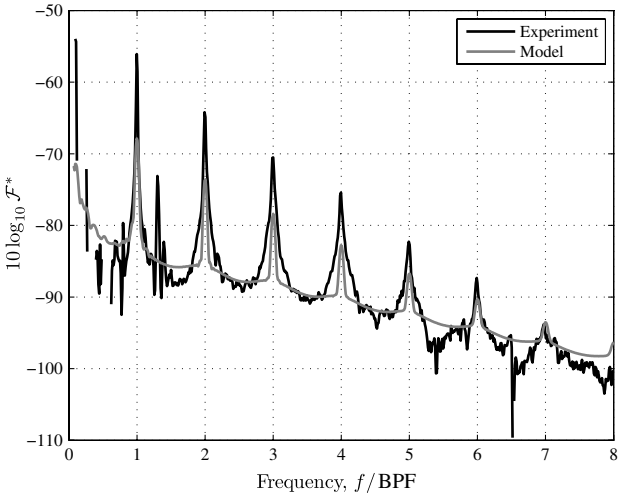


**Fig. 12 Comparison of theoretical prediction and experimentally determined unsteady lift on rotor blades due to boundary-layer turbulence. Prediction corresponds to rotor location where two-point velocity measurements were made. Rotor shaft rate = 67 Hz, $L_1/D = 1.125$, $\theta = 0.82$ mm.**

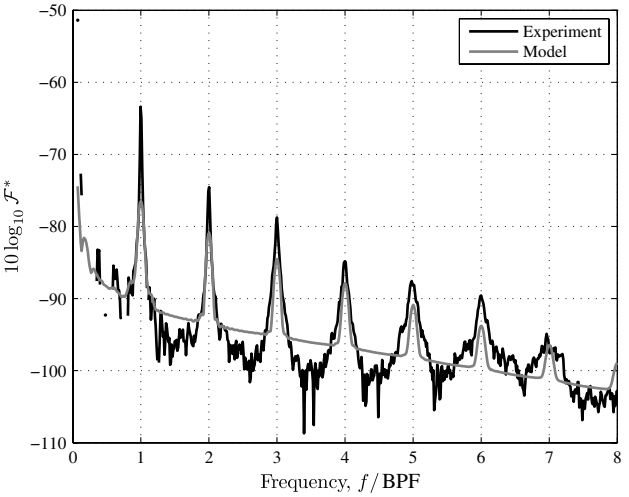


**Fig. 13 Comparison of theoretical prediction and experimentally determined unsteady lift on rotor blades due to boundary-layer turbulence. Prediction is an extrapolation from measured turbulence data. Rotor shaft rate = 67 Hz, $L_1/D = 0.25$, $\theta = 0.49$ mm.**

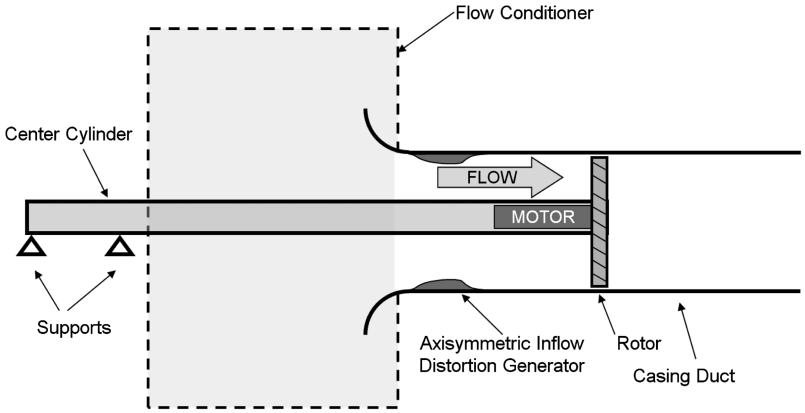


**Fig. 14 Schematic of ducted rotor model with axisymmetric inflow distortion device. Sketch not to scale.**

The resulting sound source prediction based on Eq. (10) and the turbulence statistics discussed in Sec. IV is shown in Fig. 12. Overall, the prediction is found to agree quite well with the measured sound, capturing both narrowband and wideband features. The blade-rate tones are correctly captured as having a noticeable frequency width, and decrease in magnitude with increasing order. The parameters in this case are a shaft rate equal to 67 Hz and $L_1/D = 1.125$, which correspond precisely to the inflow conditions at which the boundary-layer measurements were made. The mean error between the first and sixth blade passing frequencies was found to be 2.2 dB. The maximum error occurs at the first blade-rate tone, which is underpredicted by 12 dB, although all the blade-rate tones are underpredicted. The large-scale trend of the prediction matches the data quite well, with the broadband noise between blade-rate tones essentially predicted correctly. As a point of emphasis, the model for the two-point correlation was found based on a best match to the turbulence measurements, rather than matching the sound prediction.

The magnitude and spectral form of the rotor sound prediction shown in Fig. 12 is directly related to the specific nature of the ingested turbulence. The present authors believe that an improved model of the correlation function would lead to a more accurate sound prediction, because the measured correlation contours suggest a more complicated structure than captured in Eq. (14). For example, the measured spanwise–streamwise correlation contour features a slightly negative region for small time delays and small probe separations. This is not captured in the present model. Similarly, the measured blade-rate tones decrease in magnitude with increasing order, while increasing in width. This behavior is not captured by the present model. The specific complexities of the turbulence statistics are likely the source of the deficiencies in the sound prediction.

### A. Additional Boundary-Layer Noise Prediction

With these acoustic prediction tools developed, other rotor noise cases could be modeled. Acoustic measurements were available for the case with the rotor at $L_1/D = 0.25$. The boundary layer was thinner for this case, with $\theta = 0.49$ mm. Two-point velocity measurements were not made at this location, and the same autocorrelation functions were used as in the $L_1/D = 1.125$ case, but scaled with $\theta$. This sound prediction is therefore an extrapolation from the measured quantities. The results are shown in Fig. 13. Note that the sound measurement is an average of 7.6 dB lower than the $L_1/D = 1.125$ case between the first and sixth blade rates. The mean error between the first and sixth blade rates is 2.8 dB, demonstrating that the model largely accounts for the change in turbulence level. As can be seen, the agreement with the tones is much closer, while the broadband level between tones is overpredicted. The decay rate of the tones is reasonably well captured. The overall prediction is quite reasonable, suggesting the turbulence is well approximated by Eq. (14) and the boundary-layer correlation contours scale with $\theta$.

### B. Inflow Distortion Noise Prediction

The ingestion noise experiment and sound prediction method were tested with a modified inflow turbulence condition. Specifically, an axisymmetric inflow distortion was created using an annular revolution of a smoothed backward-facing step, a specific geometry[‡] sometimes referred to as the "NASA hump." This geometry was made as a short, 76-cm-length section of duct using rapid prototyping, with a hump height of 8.7 mm. The purpose of this geometry was to create significant inflow turbulence without the turbulence generator itself creating additional noise. The inlet distortion was placed immediately downstream of the inlet to the duct, and the rotor was positioned $0.5D$ (11.5 hump heights) downstream of the end of the inlet distortion section, as illustrated in Fig. 14.

A radial velocity survey was made using a single sensor hot-wire probe at the location of the rotor in a similar manner to the boundary-layer measurements described previously, however, two-point velocity correlation measurements were not made. The objective was to find out if using the specific values of $\theta$ and $R^*_{uu}(\tau, z_{\text{ref}})$ measured in the wake of the annular hump would be sufficient to adapt the two-point correlation model to the experiment with inflow distortion. In the case with inflow distortion, $\theta$ was found to be 2.3 mm, compared with up to 0.82 mm for the turbulent boundary layer. The variance as a function of wall-normal distance is shown in Fig. 15 and was found to have a peak value of approximately twice that of the boundary layer. It was noted that the variance again fell to zero at $z_{\text{ref}}/\theta \approx 14$.

Three autocorrelation functions were again selected to represent the inflow, shown in Fig. 16. The shapes are observed to be significantly different than those for the turbulent boundary layer, shown in Fig. 7. Specifically relevant to the radiated sound, the axial extent of the autocorrelation is much shorter, suggesting the separated flow over the hump has led to a breakup of the elongated turbulent structures. The same values of $\alpha_y$ and $\alpha_z$ found for the turbulent boundary layer were used to model the two-point cross correlation for the hump inflow, because no multisensor flow measurements were obtained for this case. The radiated rotor noise was measured using the same facility and methods described in Sec. II.

The acoustic model was evaluated for the annular hump inflow. The sound source measurement and prediction are shown in Fig. 17. The model was found to capture the overall features reasonably well, including the broad humps in the sound spectrum centered around the frequency of the blade-rate tones. The tones themselves were not found in the prediction. The overall frequency-dependent slope of the broadband sound, although significantly different than the case of boundary-layer ingestion noise, was captured quite well. Note that the overall radiated sound was 8 dB louder with the inflow distortion than the boundary-layer inflow case with $L_1/D = 1.125$. This result is seen as significant validation of both the acoustic source model

[‡]Data available online at http://cfdval2004.larc.nasa.gov/case3geometry.html.

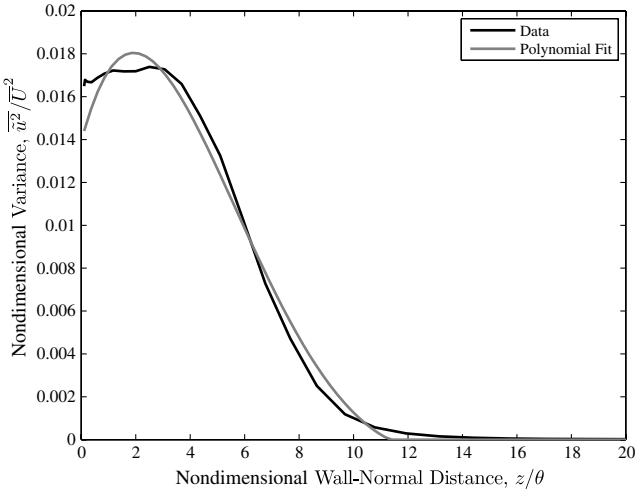


**Fig. 15 Variance of axial velocity downstream of annular hump along with polynomial fit.**

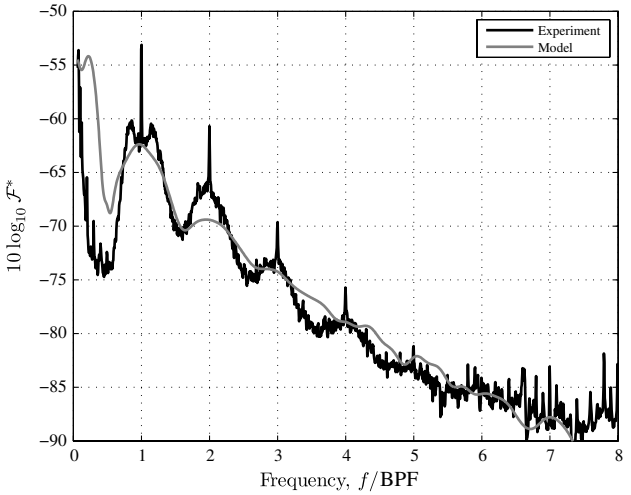


**Fig. 17 Sound source prediction for rotor ingesting inflow distortion caused by annular hump.**

given in Eq. (9) and the approximation for the two-point correlation function given in Eq. (14).

## VI. Conclusions

The sound generated by a rotor interacting with a casing turbulent boundary layer has been investigated experimentally, and an analytical method for predicting this noise has been developed. A carefully designed experiment provided a way to isolate this sound source using radiated sound measurements. The experiment was operated at a range of rotor tip speeds and a range of boundary-layer momentum thicknesses. An extension of the well-known gust response equation provided a method to predict rotor noise due to interaction with inhomogeneous and nonisotropic turbulence. A limited set of two-point velocity correlation measurements in the turbulent boundary layer provided insight into the development of a four-dimensional model for the evaluation of the sound prediction.

Two major conclusions can be drawn from the work presented here. First, a ducted rotor can generate significant blade-rate sound in the absence of mean velocity distortions due to interaction of the rotor blades with elongated turbulent structures in the casing boundary layer. These structures are of large enough axial length to interact with many rotor blades, producing correlated sound at the blade passing frequency. These tones could contribute significantly to the total sound generated by a ducted rotor system. Secondly, a space–time representation of the boundary-layer turbulence was found to provide a convenient approach to predicting this source of interaction noise. This representation is well suited to describe inhomogeneous and nonisotropic turbulent flows. Acoustic predictions for a rotor interacting with a casing boundary layer, as well as with an axisymmetric inflow distortion, were found to agree reasonably well with experimental measurements.

## Appendix: Simplification for Isotropic Turbulence

Equation (8) can be reduced to expressions found in the literature by assuming the ingested turbulence is homogeneous and isotropic, and that the turbulence is uncorrelated between rotor blades. Each blade can be considered separately, because the cross-correlation terms are zero. Under these conditions, $R_{ww} = 0$ for $m \neq n$, and the double sum can be replaced with $B$, giving

$$[\Phi_{FF}(\omega)]_{\text{rotor}} = B\beta^2(\omega) \iint \Phi_{ww}(s, s', \omega)\, \mathrm{d}s'\, \mathrm{d}s$$

Because the specific values of $s$ and $s'$ do not matter, redefine the blade span location in terms of a single location $s$ and a separation distance $\Delta s$. Of course, under the assumption of homogeneity, $\Phi_{ww}$ will be a function of separation $\Delta s$ only, and not the specific location $s$, giving

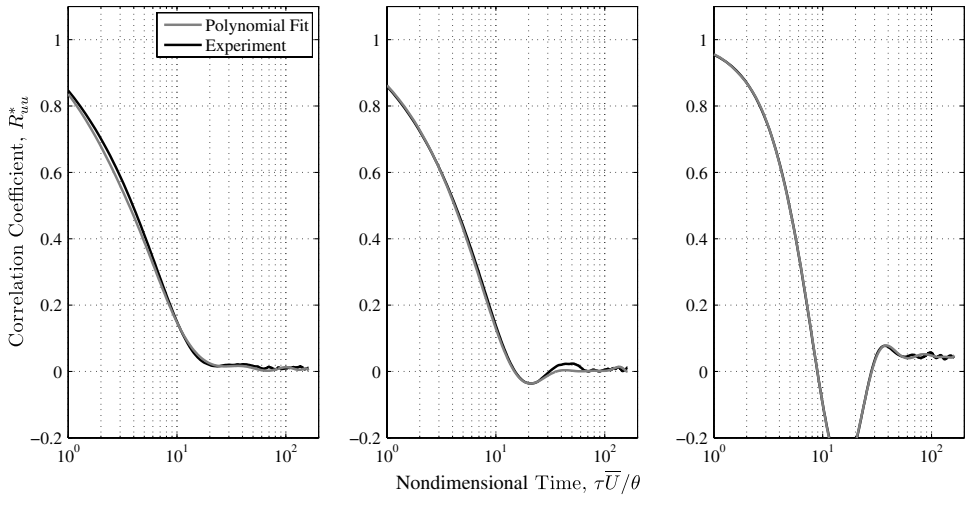


**Fig. 16 Autocorrelation functions normalized as $R^*_{uu}(\tau, z_{\text{ref}})$ measured $0.5D$ downstream of annular hump: a) $z_{\text{ref}} = 0.58$, b) $z_{\text{ref}} = 3.70$, c) $z_{\text{ref}} = 13.0$.**

$$[\Phi_{FF}(\omega)]_{\text{rotor}} = B\beta^2(\omega) \iint \Phi_{ww}(\Delta s, \omega)\, \mathrm{d}\Delta s\, \mathrm{d}s$$

Multiply and divide by the single point autocorrelation of axial velocity $\Phi_{ww}(\omega)$ to get

$$[\Phi_{FF}(\omega)]_{\text{rotor}} = B\beta^2(\omega) \iint \Phi_{ww}(\omega) \frac{\Phi_{ww}(\Delta s, \omega)}{\Phi_{ww}(\omega)}\, \mathrm{d}\Delta s\, \mathrm{d}s$$

Use the definition of the spanwise integral length scale

$$2\Lambda_s(\omega) \equiv \int_{-\infty}^{\infty} \frac{\Phi_{ww'}(\omega)}{\Phi_{ww}(\omega)}\, \mathrm{d}\Delta s$$

and assume that the scale of the turbulence is small enough with respect to the airfoil span that the infinite integral can be approximated with an integral over the blade span. The second integral gives $\int \mathrm{d}s = S$, where $S$ is the blade span, resulting in

$$[\Phi_{FF}(\omega)]_{\text{rotor}} = 2SB\beta^2(\omega)\Phi_{ww}(\omega)\Lambda_s(\omega) \tag{A1}$$

In the case of $B = 1$, this equation is identically equal to the expression presented as Eq. 7 of Minitti et al. [28].

## Acknowledgments

The authors would like to thank Ki-Han Kim and Debbie Nalchajian of the U.S. Office of Naval Research for support of this project.

## References

[1] Blake, W. K., *Mechanics of Flow-induced Sound and Vibration (two volumes)*, Vols. 1–2, Academic Press, New York, 1986.

[2] Wright, S. E., "The Acoustic Spectrum of Axial Flow Machines," *Journal of Sound and Vibration*, Vol. 45, No. 2, 1976, pp. 165–223. doi:10.1016/0022-460X(76)90596-4

[3] Morfey, C. L., "Rotating Blades and Aerodynamic Sound," *Journal of Sound and Vibration*, Vol. 28, No. 3, 1973, pp. 587–617. doi:10.1016/S0022-460X(73)80041-0

[4] Huff, D. L., "Fan Noise Prediction: Status and Needs," NASA TM-97-206533, 1998.

[5] Hanson, D. B., "Spectrum of Rotor Noise Caused by Atmospheric Turbulence," *Journal of the Acoustical Society of America*, Vol. 56, No. 1, 1974, pp. 110–126. doi:10.1121/1.1903241

[6] Moiseev, N., Lakshminarayana, B., and Thompson, D. E., "Noise Due to Interaction of Boundary-Layer Turbulence with a Compressor Rotor," *Journal of Aircraft*, Vol. 15, No. 1, 1978, pp. 53–61. doi:10.2514/3.58312

[7] Ganz, U. W., Joppa, P. D., Patten, T. J., and Scharpf, D. F., "Boeing 18-Inch Fan Rig Broadband Noise Test," NASA CR-1998-208704, 1998.

[8] Glegg, S., and Walker, N., "Fan Noise from Blades Moving Through Boundary Layer Turbulence," *5th AIAA/CEAS Aeroacoustics Conference*, AIAA Paper 99-1888, May 1999.

[9] Joseph, P., and Parry, A., "Rotor/Wall Boundary-Layer Interaction Broadband Noise in Turbofan Engines," *7th AIAA/CEAS Aeroacoustics Conference*, AIAA Paper 2001-2244, May 2001.

[10] Martinez, R., "Broadband Sources of Structure-Borne Noise for Propulsors in 'Haystacked' Turbulence," *Computers and Structures*, Vol. 65, No. 3, 1997, pp. 475–490. doi:10.1016/S0045-7949(96)00261-1

[11] Atassi, H. M., and Logue, M. M., "Fan Broadband Noise in Anisotropic Turbulence," *15th AIAA/CEAS Aeroacoustics Conference*, AIAA Paper 2009-3148, May 2009.

[12] Sevik, M., "Sound Radiation from a Subsonic Rotor Subjected to Turbulence," Pt. 2, *Fluid Mechanics, Acoustics, and Design of Turbomachinery*, NASA SP-304 1974, pp. 493–511.

[13] Stephens, D. B., and Morris, S. C., "A Method for Quantifying the Acoustic Transfer Function of a Ducted Rotor," *Journal of Sound and Vibration*, Vol. 313, Nos. 1–2, 2008, pp. 97–112. doi:10.1016/j.jsv.2007.11.054

[14] Gliebe, P., "Observations on Fan Rotor Broadband Noise Characteristics," AIAA Paper 2004-2909, May 2004.

[15] Bendat, J. S., and Piersol, A. G., *Random Data, Analysis and Measurement Procedures*, Wiley, New York, 2000.

[16] Kovasznay, L. S. G., Kibens, V., and Blackwelder, R. F., "Large-Scale Motion in the Intermittent Region of a Turbulent Boundary Layer," *Journal of Fluid Mechanics*, Vol. 41, No. 2, 1970, pp. 283–325. doi:10.1017/S0022112070000629

[17] Ganapathisubramani, B., Hutchins, N., Hambleton, W. T., Longmire, E. K., and Marusic, I., "Investigation of Large-Scale Coherence in a Turbulent Boundary Layer Using Two-Point Correlations," *Journal of Fluid Mechanics*, Vol. 524, 2005, pp. 57–80. doi:10.1017/S0022112004002277

[18] Krogstad, P. A., and Antonia, R. A., "Structure of Turbulent Boundary Layers on Smooth and Rough Walls," *Journal of Fluid Mechanics*, Vol. 277, 1994, pp. 1–21. doi:10.1017/S0022112094002661

[19] Zhou, J., Adrian, R. J., and Balachandar, S., "Autogeneration of Near-Wall Vortical Structures in Channel Flow," *Physics of Fluids*, Vol. 8, No. 1, 1996, pp. 288–290. doi:10.1063/1.868838

[20] Adrian, R. J., Meinhart, C. D., and Tomkins, C. D., "Vortex Organization in the Outer Region of the Turbulent Boundary Layer," *Journal of Fluid Mechanics*, Vol. 422, 2000, pp. 1–54. doi:10.1017/S0022112000001580

[21] Hutchins, N., and Marusic, I., "Evidence of Very Long Meandering Features in the Logarithmic Region of Turbulent Boundary Layers," *Journal of Fluid Mechanics*, Vol. 579, 2007, pp. 1–28. doi:10.1017/S0022112006003946

[22] Amiet, R. K., "On the Second-Order Solution to the Sears Problem for Compressible Flow," *Journal of Fluid Mechanics*, Vol. 254, 1993, pp. 213–228. doi:10.1017/S0022112093002095

[23] Amiet, R. K., "High Frequency Thin-Airfoil Theory for Subsonic Flow," *AIAA Journal*, Vol. 14, No. 8, 1976, pp. 1076–1082. doi:10.2514/3.7187

[24] Liepmann, H. W., "Extension of the Statistical Approach to Buffeting and Gust Response of Wings of Finite Span," *Journal of the Aeronautical Sciences*, Vol. 22, 1955, pp. 197–200.

[25] Howe, M. S., *Acoustics of Fluid-Structure Interactions*, Cambridge Univ. Press, Cambridge, England, U.K., 1998.

[26] Glegg, S. A. L., "The Response of a Swept Blade Row to a Three-Dimensional Gust," *Journal of Sound and Vibration*, Vol. 227, No. 1, 1999, pp. 29–64. doi:10.1006/jsvi.1999.2327

[27] Atassi, H., Ali, A., Atassi, O., and Vinogradov, I., "Scattering of Incident Disturbances by an Annular Cascade in a Swirling Flow," *Journal of Fluid Mechanics*, Vol. 499, 2004, pp. 111–138. doi:10.1017/S0022112003007031

[28] Minniti, R. J., Blake, W. K., and Mueller, T. J., "Inferring Propeller Inflow and Radiation from Near-Field Response, Part 1: Analytic Development," *AIAA Journal*, Vol. 39, No. 6, 2001, pp. 1030–1036. doi:10.2514/2.1443

S. Fu
*Associate Editor*